ADVANCED MATERIALS INTERFACES
www.advmatinterfaces.de

Repulsion of Polar Gels From Water: Hydration-Triggered Actuation, Self-Folding, and 3D Fabrication

Inam Ridha, Pranvera Gorenca, Russell Urie, Sachin Shanbhag, and Kaushal Rege**

Synthetic materials that mimic the ability of natural occurring features to self-actuate in response to different stimuli have wide applications in soft robotics, microdevices, drug delivery, regenerative medicine, and sensing. Here, unexpected and counter-intuitive findings are presented in which a strongly polyelectrolytic hydrogel repels from strong polar solvents upon partial exposure (e.g., partial hydration by water). This repulsion drives the actuation and self-folding of the gel, which results in rapid formation of different three-dimensional shapes by simply placing the corresponding two-dimensional films on water. A detailed investigation into the role of hydrogel chemistry, pH, and morphology on hydration-triggered actuation behavior of the gels and their nanocomposites is described. Finally, a computational model is developed in order to further elucidate mechanisms of actuation. Modeling partial hydration as a repulsive driving force, it tracks the evolution of the shape of the thin film that results from restoring elastic forces. Taken together, the results indicate that an interplay between elastic and Coulombic repulsive forces leads to seemingly unexpected behavior of actuation of strongly polyelectrolytic gels away from polar solvents, leading to a novel and simple fabrication strategy for diverse 3D devices.

1. Introduction

Folded structures, including pine cones,[1–3] intestinal villi, and blood vessels[4] are ubiquitous in nature. Synthetic materials that mimic naturally occurring folded structures and demonstrate actuation and folding in response to external triggers, have several applications in robotics,[5] microdevices,[6,7] drug delivery,[8,9] cell culture,[10] surgery,[11,12] and sensing technologies.[13–15] A wide range of external stimuli including changes in temperature,[8,11,16–19] electrical field,[13] light,[12,13,20,21] pH,[8,14,21] hydration and humidity,[3,22] solvent composition,[8,18,23] and ion composition[15,20] can be used to trigger responses in synthetic materials. Diverse fabrication methods including cutting,[14,24,25] molding, imprinting,[16] or photolithography[13,16,19,24,26] have been used to generate diverse 3D structures including tubes, capsules, cubes,[6–9] and pyramids that are responsive to such stimuli.[27]

Most self-folding polymers or films are typically based on gradients or spatial heterogeneities, that are engineered in order to create environmentally responsive changes in their morphology.[7,16,19,28,29] Such strategies mostly consist of generating different cross-linking gradients along the thickness or lateral dimension of polymer films,[25,29] designing polymer bilayers or multilayers with different degrees of swelling,[3,14,22,27,29,30] or depositing a polymer layer on top of a nonpolymeric material,[14,21] all of which result in thin heterogeneous, stimuli-responsive sheets.

Here, we report hydration-triggered activation of a single-component cationic hydrogel, "Amikagel,"[31,32] derived from an aminoglycoside antibiotic, amikacin (AM), cross-linked with diglycidyl ethers. The hydrogel is homogeneous in that no gradients of cross-linking or porosity are intentionally engineered into its morphology. The polar hydrogel undergoes immediate and reversible folding upon partial wetting by aqueous solutions, which, at first look, is counter-intuitive considering the system involves repulsion of a cationic polyelectrolytic gel from a strongly polar solvent (water). The folding behavior of this cationic hydrogel was strongest at acidic pH but was lost at conditions of highly basic pH. Conjugation of acidic amino acids to the gel resulted in reduced efficacy of hydration-triggered folding. The actuation behavior was maintained even upon the incorporation of metallic nanoparticles (gold nanorods, GNRs) within the hydrogel matrix.[33] We demonstrate the actuation behavior for different morphologies of the hydrogel, resulting in the formation of diverse and complex 3D shapes, which allow for design and hydration-triggered fabrication of a variety of constructs in biotechnology, energy devices, and sensors.

I. Ridha
Biomedical Engineering
Arizona State University
Tempe, AZ 85287, USA
P. Gorenca
Materials Science and Engineering
Arizona State University
Tempe, AZ 85287, USA
Dr. R. Urie,[+] Prof. K. Rege
Chemical Engineering
Arizona State University
Tempe, AZ 85287, USA
E-mail: rege@asu.edu
Prof. S. Shanbhag
Department of Scientific Computing
Florida State University
Tallahassee, FL 32306, USA
E-mail: sshanbhag@fsu.edu
The ORCID identification number(s) for the author(s) of this article can be found under https://doi.org/10.1002/admi.202000509.
[+]Present address: Department of Biomedical Engineering, University of Michigan, Ann Arbor, MI 48109, USA

DOI: 10.1002/admi.202000509

2. Experimental Section

2.1. Materials

Amikacin hydrate, poly(ethylene glycol) diglycidyl ether (PEGDE; M_n = 500), 1,4-butanediol diglycidyl ether (BDDE; M_n = 202), and poly(ethylene glycol) methyl ether thiol (M_n = 5000), Boc-protected aspartic acid, gold (III) chloride trihydrate ($HAuCl_4 \cdot 3(H_2O)$), cetyltrimethylammonium bromide (CTAB), L-ascorbic acid, sodium borohydride ($NaHB_4$), silver nitrate ($AgNO_3$), 1-ethyl-3-(3-dimethylaminopropyl) carbodiimide (EDC), *N*-hydroxysuccinimide (NHS), sodium hydroxide, hydrochloric acid, dimethyl sulfoxide (DMSO), and dimethylformamide (DMF) were purchased from Sigma-Aldrich and used without any further purification.

2.2. Hydrogel Formation

A pre-gel solution was prepared by dissolving amikacin hydrate (100 mg; 170 $\times 10^{-3}$ M) in 1 mL nanopure water (NPW; resistivity ≈18.2 MΩ cm, Millipore filtration system, Darmstadt, Germany), and a threefold molar excess of PEGDE (224 µL of M_n = 5000 stock) or BDDE (176 µL of M_n = 200 stock) as the cross-linking agents. The mixture was cast in glass-bottomed 35 mm cell culture dishes after being vortexed for about 1 min in order to obtain a uniform solution. The hydrogels, formed after 8 h, were named AM-PEGDE and AM-BDDE following polymerization of AM with PEGDE, and BDDE, respectively. To generate Amikagel nanocomposites incorporated with GNRs, PEGylated GNRs (described below) were centrifuged and added to the pre-gel solution resulting in a final GNR concentration of 1 wt%. The pre-gel solution was poured into 6-well plates and the plate was kept at room temperature overnight in order to allow the formation of Amikagel-GNR nanocomposites.

2.3. Generation of GNRs

GNRs were synthesized using a seedless method adopted from literature.[34] Briefly, gold(III) chloride trihydrate ($HAuCl_4 \cdot 3H_2O$) (20 mL, 1×10^{-3} M) was added to 20 mL of an aqueous solution of CTAB (0.2 M), followed by the addition of 300 µL of $AgNO_3$ (4.0×10^{-3} M). Next, 12 µL of HCl (37% v/v in water) was rapidly added to the solution to obtain a pH of ≈11, following which, ascorbic acid (75 µL of 85.8×10^{-3} M) was added to the solution. After the solution became clear, 7.5 µL of $NaBH_4$ (0.01 M) was immediately injected into the solution. The gold nanoparticles were allowed to mature overnight and resulting CTAB-templated GNRs were purified three times by centrifugation (9000 g, 10 min).

2.4. PEGylation of GNRs

PEGylation, i.e., conjugation with poly(ethylene glycol) or PEG, of CTAB-templated GNRs was carried out using protocols described in the literature.[35] Briefly, mPEG5000-SH (PEG-SH; 3 mg) was added to a dispersion of GNRs (1 mL; OD = 0.5) in nanopure water and allowed to mix overnight at room temperature. The GNR dispersion was centrifuged at 14 000 rpm for 10 min in order to remove unreacted PEG-SH molecules. The precipitate was resuspended in nanopure water in order to obtain PEGylated GNRs. PEGylated GNRs were added to Amikagels at weight percentages of 1% w/v resulting in the formation of AM-PEGDE-GNR nanocomposites.

2.5. Hydration-Triggered Actuation of Amikagel Films

AM-PEGDE films were cut into X-shapes, mechanical wheels, gears, triangles, rectangles, and squares, and placed on the surface of nanopure water in cell culture dishes (40 mm diameter) at room temperature in order to allow partial wetting at the bottom surface of the film. Hydration-triggered actuation of these films was recorded with Canon EOS 1100 DSLR camera over a period of 1–2 min until the samples reached their maximum folding. The sample was then removed from the liquid, placed on dry paper, and photographed using Canon a EOS 1100 DSLR camera. Actuation of Amikagel films prepared using a different cross-linker (BDE) and Amikagel-GNR nanocomposites was also carried out in a similar manner. In all cases, the time required for maximum folding and the ratio of the surface area at maximum folding normalized to the original surface area were determined.

2.6. Determination of Amikagel Swelling Ratio

Circular disc shaped Amikagel (AM-PEGDE) films, approximately ≈150 mg in initial weight and 2 cm diameter, were placed on the surface of nanopure water for 1 min. The sample was then removed, weighed and placed on dry paper for 5 min, and was weighed again. This cycle repeated for five times. The swelling ratios of the films were measured after each cycle in which, the swelling of each sample was calculated by subtracting the weight of swollen gel from the weight of initial dry gel. This number was normalized to the weight of the initial dried sample in order to obtain the swelling ratio as shown below.

$$\text{Swelling Ratio} = \frac{M_{\text{wet}} - M_{\text{dry}}}{M_{\text{dry}}} \times 100 \quad (1)$$

where M_{wet} is the weight of the swollen gel, and M_{dry} is the weight of the initial dry gel.

2.7. Effect of pH on Amikagel Actuation

Five solutions with different pH values, 2, 5, 7, 10 and 12, were prepared using 1 M NaOH solution and 1 M HCl solution, and the pH values of the stock solutions were determined using a pH meter. The solution (1 mL) was added to individual cell culture plates and circular or semicircular AM-PEGDE, AM-BDE, and AM-PEGDE-GNR films were placed on top of these solutions. The pH-dependent actuation response was recorded using a Canon EOS T6 camera. A screenshot from the video

was acquired every 5–10 s and the area of the Amikagel film was calculated using ImageJ. The surface area at each time was normalized to the initial area of the film (before actuation) in order to obtain the surface area ratio at each time point, resulting in temporal profiles of the actuation behavior.

2.8. Effect of Film Thickness on Actuation

Fifteen different circular disk-shaped AM-PEGDE gel with thicknesses ranging from 0.3 to 0.52 mm were prepared; film thickness was determined using a digital caliper. Each AM-PEGDE film was placed on the surface of nanopure water, and the time required for each sample to reach its final folded configuration was recorded. This time was plotted as a function of film thickness.

2.9. Conjugation of Amino Acids to Amikagels

Amikagels were derivatized with aspartic acid in order to investigate the effect of a reduced number of amines on hydration-triggered actuation of the hydrogel. Briefly, Boc-protected aspartic acid (0.25×10^{-3} M), which contains two free carboxyl groups, was reacted with primary amines in both Amikagel films using well-established EDC-NHS chemistry. This reaction results in the formation of amide bonds between the amines of the Amikgel and the carboxylic acids in aspartic acid. For each sample of Amikagel generated using 100 mg (0.05×10^{-3} M) amikacin in the polymerization reaction, an excess equivalent of aspartic acid (0.25×10^{-3} M), EDC (0.4×10^{-3} M), and NHS (0.4×10^{-3} M) were added to 2 mL DMF for 48 h at 37 °C. Following derivatization, the samples were washed with DMSO and water and dried in an incubator oven at 37 °C temperature. The Boc group was not removed from the derivatized Amikagels in order to maintain a lower amount of amines (because of the conjugation). Amikagel derivatization with aspartic acid was verified using potentiometric titration.

2.10. Potentiometric Titration of Amikagel Films

Potentiometric titration[36,37] was carried out in order to determine the ionization constant of parental and conjugated Amikagels as an indicator of the conjugation of the amino acid. The pH of nanopure water (10 mL) was adjusted between 10 and 11 by adding 0.01 M NaOH. Amikagel (40 mg) was added to this solution and titrated against 0.01 M HCl at room temperature under continuous stirring. Sufficient time (10 min) was allowed for attaining equilibrium after each instance of HCl addition under continuous stirring. Both, pH of the solution and the volume of added HCl were recorded in order to obtain the curve which describes the relationship between the degree of ionization and pH. The reference curve was obtained using the same method of titration and the same solution but without Amikagel. The apparent titration curve of Amikagel was obtained by subtracting the reference titration curve from that of the Amikagel curve. The ionization degree of the polymer, α, was calculated as $(N - n)/N$ (shown below), where n is the number of moles of HCl required to achieve the desired pH value (at each data point) and N is the total number of moles of HCl required for titration of the Amikagel sample.[36]

$\alpha = (N - n)/N$

n = HCl moles/ΔpH

N = total HCl moles/sample

pK_a which is the negative base-10 logarithm of the acid dissociation constant (K_a) was determined from the Henderson–Hasselbalch equation by plotting α versus pH as indicated below:

$$\mathrm{pH} = \mathrm{p}K_a + \log\left(\frac{\alpha}{1-\alpha}\right) \tag{2}$$

2.11. Statistical Analyses

Statistical analyses were carried out using one-way ANOVA and Tukey test. In all cases, $n = 6$ independent experiments were carried out unless otherwise indicated and statistical significance is indicated by $^{*}p$-values < 0.05, $^{**}p$-values < 0.01, $^{***}p$-values < 0.001, and $^{****}p$-values < 0.0001 compared to the respective control.

2.12. Computational Model

Deformation of polymer or polyelectrolyte gels arises fundamentally from a competition between osmotic and elastic forces. Depending on the resolution desired and properties of interest, modeling strategies for polyelectrolyte gels range from statistical theory,[38] multifield formulations,[39,40] to molecular simulations.[41] In statistical theory, the total free energy of the system is made up of contributions from mixing, elastic deformation, and mobile ion phases. It is useful when the focus is on global mechanical properties, e.g. swelling ratio in hydrogels. Multifield formulations consider coupled differential equations that model chemical (transport/diffusion of species), electrical (Poisson equation), and mechanical (momentum balance) fields. This level of modeling provides local information, and is useful for quasi-static or transient problems. A detailed micromechanical model (discrete element formulation) may be combined with this strategy[40] to deal with large deformations and strains. In molecular simulations,[41,42] ions are explicitly resolved as charge-bearing hard spheres undergoing Coulombic interactions, while polymer strands are resolved using a bead-spring model.

In this work, the focus is on solvent-mediated shape change. Therefore, we consider a simplified 2D computational model for the cross-section of the thin film gel. The deformation of the film is modeled as a competition between elastic and repulsive interactions. Elasticity is modeled by a sequence of N rectangular cells, as shown in **Figure 1**. Edges of these cells are modeled as Hookean springs. Springs are connected by point particles arranged in two rows. The elastic spring energy between connected particles i and j, located at $\mathbf{r}_i$ and $\mathbf{r}_j$ is given by

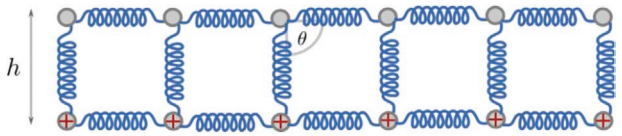

Figure 1. Schematic diagram of the cross-section of an elastic thin film with $N = 5$ cells. Particles are shown in gray. The lower layer is charged at time $t = 0$, and the subsequent evolution of the shape of the film is tracked.

$$E_{ij}^{s} = k_s(|r_{ij}| - l_s)^2 \tag{3}$$

where $|\mathbf{r}_{ij}|$ is the distance between the particles, k_s is the spring constant, and l_s is the equilibrium length of the spring. The shape of the elastic cells is maintained through an elastic angular bending potential,

$$E_{ijk}^{a} = k_\theta \left(\theta_{ijk} - \theta_0\right)^2 \tag{4}$$

where θ_{ijk} is the angle between two adjacent bonds connected that share particle j as a common vertex (see Figure 1). Deviations from rectangular geometry for individual cells are penalized by setting $\theta_0 = \pi/2$. We model the protonation of amine groups upon hydration by asserting that the particles in the lower layer of the thin film acquire a small net charge at time $t = 0$. The resulting electrostatic repulsion is modeled by a Coulomb-like repulsive force,

$$E_{ij}^{r} = \frac{q^2}{|r_{ij}|} \tag{5}$$

where q is the net charge on each particle in the lower layer. Note that this electrostatic repulsion is a convenient proxy for the more complicated process of counterion transport driven by osmotic pressure difference between the gel and the solvent. Counterion transport is known to cause swelling in polyelectrolyte hydrogels immersed in water. However, resolving it explicitly requires much more detailed modeling.[41,42] A repulsive force like the inverse square law above, that acts along a pair of connected particles approximates this process.

The force on particle i due to the elastic and repulsive interactions is given by the negative gradient of the potential. In addition to the elastic and repulsive forces, we add a dissipative drag force, $\mathbf{F}^{d}_{i} = \zeta \mathbf{v}_i$, to damp the harmonic oscillations that arise in networks of springs. Here ζ is the drag coefficient, and $\mathbf{v}_i$ is the velocity of particle i. The total force on particle i is the sum of the elastic and repulsive force contributions, and the drag force,

$$F_i = \sum\nolimits_j F_{ij}^{s} + \sum\nolimits_{j,k} F_{ijk}^{a} + \sum\nolimits_j F_{ij}^{r} + F_i^{d} \tag{6}$$

The first two terms on the RHS are elastic energy contributions, the third term is the repulsive interaction, and the last term is the drag force. The resulting equations of motion,

$$m\,\ddot{r}_i = F_i \tag{7}$$

are integrated using a leap-frog algorithm with timestep $\Delta t = 0.05$.[43] Initially, particles are arranged on a grid in two layers as shown in Figure 1; in the absence of repulsive forces ($q = 0$), this is the equilibrium state of the thin film, since the elastic forces are balanced.

The following parameters were considered: For particles i and j in the same layer, we set $l_s = 1$. For horizontally aligned springs connecting particles in the top (bottom) layer, we set $k_s = 2$ ($k_s = 1$). The smaller value of k_s for springs in the lower layer is designed to make them more susceptible to deformation. In hydrogels, for instance, contact of the polyelectrolyte gel with a thermodynamically compatible solvent leads to solvation of the glassy polymer to a rubbery region.[44] For vertically aligned springs we set $k_s = 2$, and $l_s = h$. The width of a cell is set to $w = 1$, and the angular force constant $k_\theta = 0.5$. In the base case, $\zeta = 1.0$ and $q = 1$. The thickness $h = 0.5$, and horizontal dimension is set to $N = 25$ cells (52 particles). The aspect ratio is thus $25/0.5 = 50$. For convenience, we assume that the mass of a particle $m = 1$, throughout. As thickness increases, the increase in structural rigidity is modeled by making k_θ proportional to thickness, h. The associated increase in inertia is modeled by making the drag ζ a function of h as well. Comparison with experimental data suggests a dependence of $\zeta \approx h^{2.5}$.

3. Results and Discussion

3.1. Hydration-Triggered Actuation of Amikagel films

Amikagel films were generated by cross-linking between amines in aminoglycoside amikacin with epoxide groups present in PEGDE or BDDE, resulting in gels that contain both amine and hydroxyl groups (Figure S1, Supporting Information).[32,45] **Figure 2** shows various 3D objects that were fabricated following hydration-triggered actuation and folding of different 2D shapes of AM-PEGDE films. After placing the film on the surface of water, each shape was seen to curl such that the actuation resulted in minimization of the contact area between the film and the water. The left column in the figure represents the original shape of the Amikagel films (AM-PEGDE), and the right column shows the final 3D shape of the films in 1 min after hydration-triggered actuation. Placing either side of the film on the solvent surface gave a similar actuation response because of the relative homogeneity of the film chemistry. Similar actuation behavior was observed with other polar solvents including ethanol and acetone, but was not seen in presence of hexane, an organic solvent (Figures S2 and S3, Supporting Information) indicating that protonation of amines (Figure S1, Supporting Information) in polar solvents is likely responsible for the actuation behavior (Figure S4, Supporting Information).

Hydration-triggered actuation and self-folding behavior of Amikagel films containing a different cross-linker, BDDE and GNR-embedded AM-PEGDE gels (AM-PEGDE-GNRs) were studied and compared with that of AM-PEGDE gels. AM-PEGDE films reached their maximum extent of folding within 60 s but AM-BDDE films required ≈300 s to reach their final folded configuration (**Figure 3**). The BDDE cross-linker is shorter in length than PEGDE, which likely restricts the

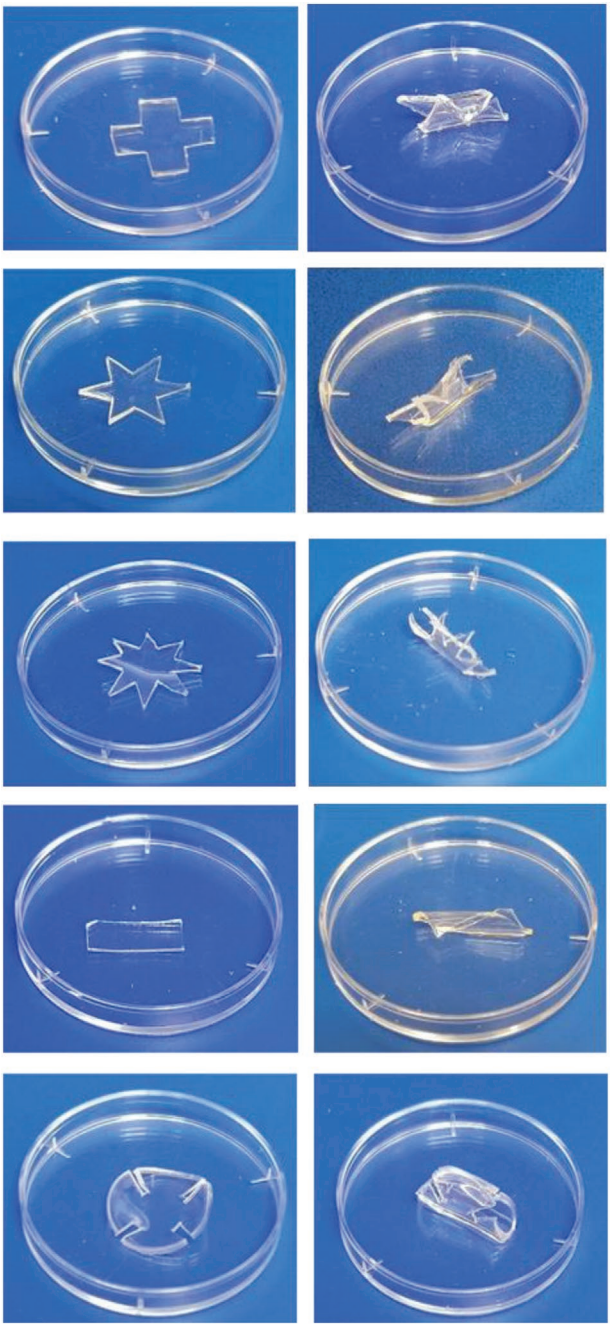

Figure 2. Left column: original shapes of AM-PEGDE films before they were placed on the surface of water. Right column: corresponding fabricated 3D structures obtained upon actuation by partial hydration of the gels for 1 min.

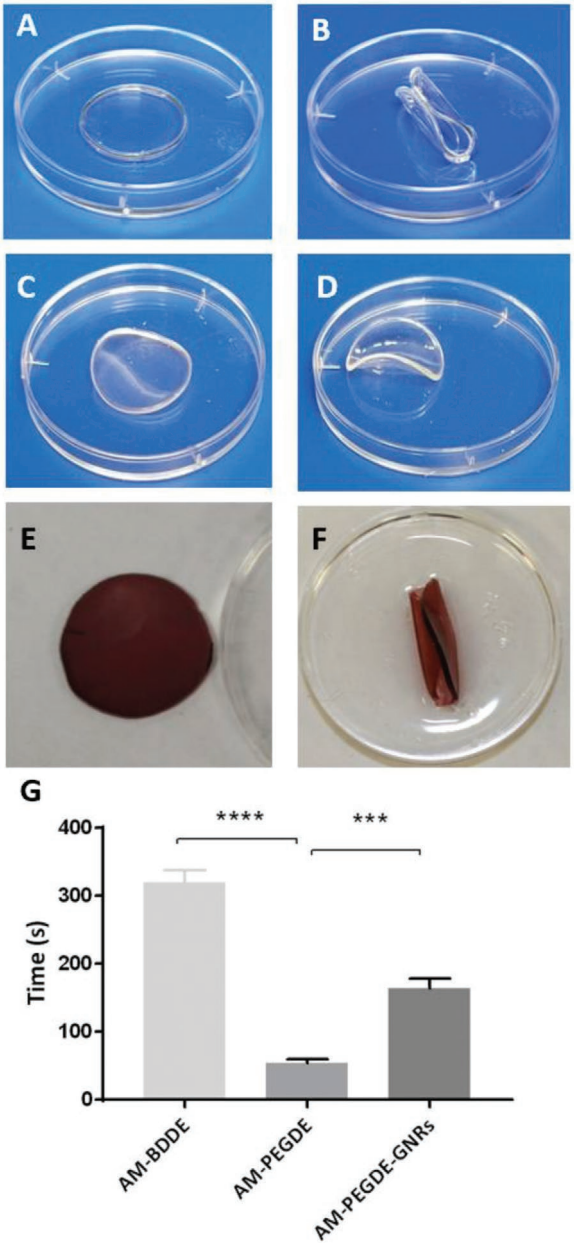

Figure 3. Hydration-triggered actuation and self-folding of different films at time $t = 0$ min (left column) and upon reaching equilibrium (right column). A,B) AM-PEGDE films, which reach 0.53 ± 0.04 of the original surface area at ≈50s. C,D) AM-BDDE films, which reach 0.72 ± 0.06 of the original surface area at ≈300 s. E,F) AM-PEGDE-GNR films, which reach 0.52 ± 0.04 of their original surface area at ≈80 s. In all cases, the figures are representative images of $n = 3$ independent experiments. G) The time required for respective films to achieve the final configuration. $^{***}p$-values < 0.001 for AM-BDDE and AM-PGDE-GNRs with respect to AM-PEGDE films.

movement of polymer chains and limits the extent and kinetics of actuation. AM-PEGDE-GNR films (1 weight% GNRs) also demonstrated hydration-triggered actuation albeit at a two- to threefold slower rate compared to parental AM-PEGDE films (Figure 3G) likely because of constraints to mobility caused by the presence of the dense metallic nanoparticles and the resulting increase in mechanical properties (modulus of toughness; Figure S5, Supporting Information).

3.2. Drying-Triggered Unfolding of Amikagel Films

Figure 4A shows hydration-triggered folding of an originally circular AM-PEGDE film in 1 min after placing on water for hydration-triggered self-folding. The tube was then placed on a dry surface, which resulted in unfolding to its near-original

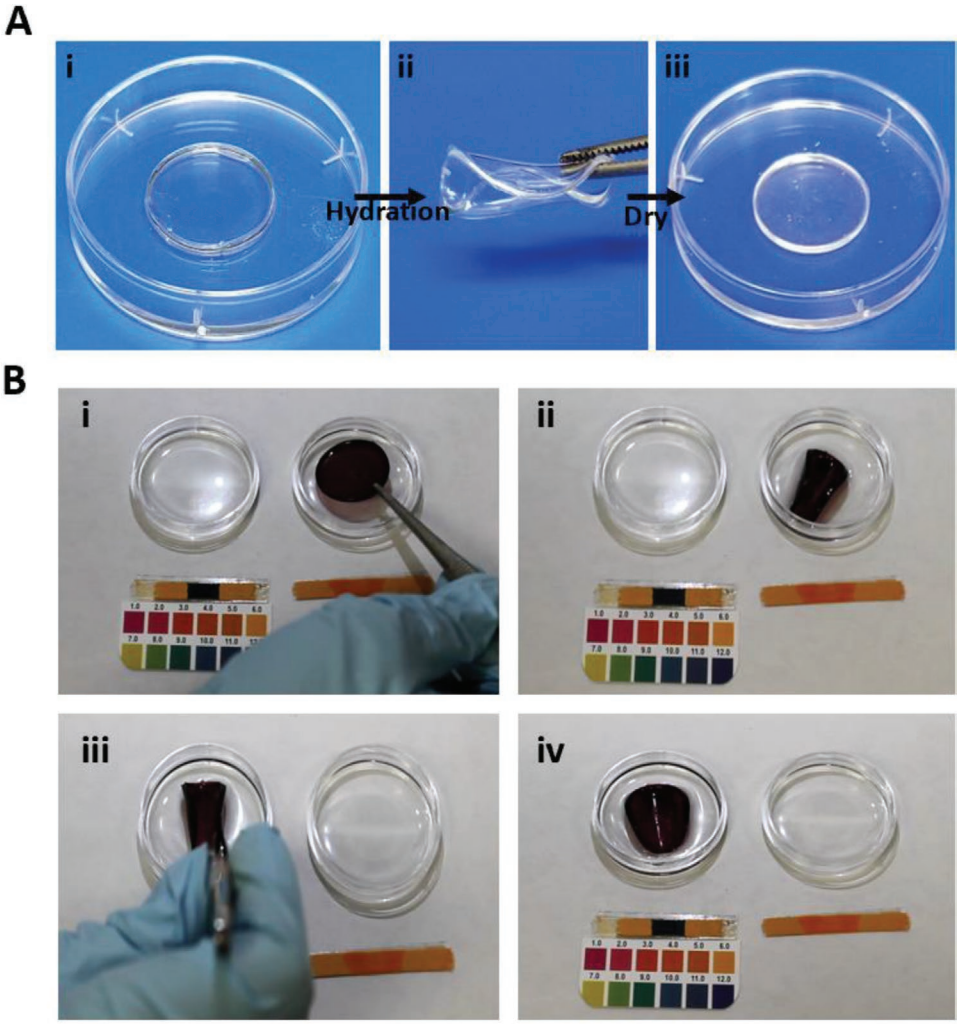

Figure 4. A) Self-folding and unfolding behavior of AM-PEGDE; i: before placing on the surface of the nanopure water, ii: immediately after the film was placed on the surface of the water for 1 min, and iii: 3 min after the folded structure in (ii) was placed on a dry surface. B) Folding of AM-PEGDE-GNR films at low pH is reversed at high pH. In all figures, the pH of the solution in the right dish is ≈5 and that in the left dish is ≈12 (indicated visually by pH strips). AM-PEGDE-GNR films (GNRs: 1 wt%) fold symmetrically in the acidic medium within 1 min. i: Immediately prior to placing the film on the pH 5 solution, ii: shape of the film 60 s after placing it on the pH 5 solution, iii: immediately before the transfer of the film from pH 5 to 12, and iv: shape of film 60 s the following transfer to the pH 12 solution.

shape after ≈3 min. In addition, it was also possible to reverse the folding of Amikagels and their nanocomposites by placing them on a highly basic (pH 12) solution (Figure 4B); the original shape was recovered in 2 min in case of the AM-PEGDE-GNR nanocomposite.

3.3. Effect of pH on Hydration-Triggered Actuation of Amikagel films

In order to investigate the effect of pH on hydration-triggered actuation and self-folding, AM-PEGDE and AM-BDDE films were placed on five different solutions with pH values ranging from 2 to 12. The folding of circular (flat) films into tubular shapes was visualized and changes in the surface area were determined as a function of pH and time. **Figure 5** shows that acidic pH (e.g., pH 2) resulted in the fastest kinetics as well as the greatest extent of folding as defined by the surface area ratio (surface area at a given time normalized to the surface area of the film before actuation); no folding was observed at pH ≈12. Consistent with previous results, AM-PEGDE demonstrated faster as well as greater folding compared to AM-PEGDE-GNR nanocomposites and AM-BDDE films at pH values less than 12 (Figure 5A–C). It is important to note that the swelling ratio of AM-PEGDE films decreased with pH (Figure S6, Supporting Information). The maximum swelling ratio was seen at pH ≈12 where the hydration-triggered actuation of the films was not observed. These results indicate that under conditions of higher pH, the hydrogels likely possess a greater propensity to absorb water and swell, but under conditions of lower pH, the partial hydration triggers actuation while minimizing swelling (Figure S6, Supporting Information). Taken together, these findings indicate that protonation of the amines at acidic pH conditions triggers the actuation and self-folding in the different gels

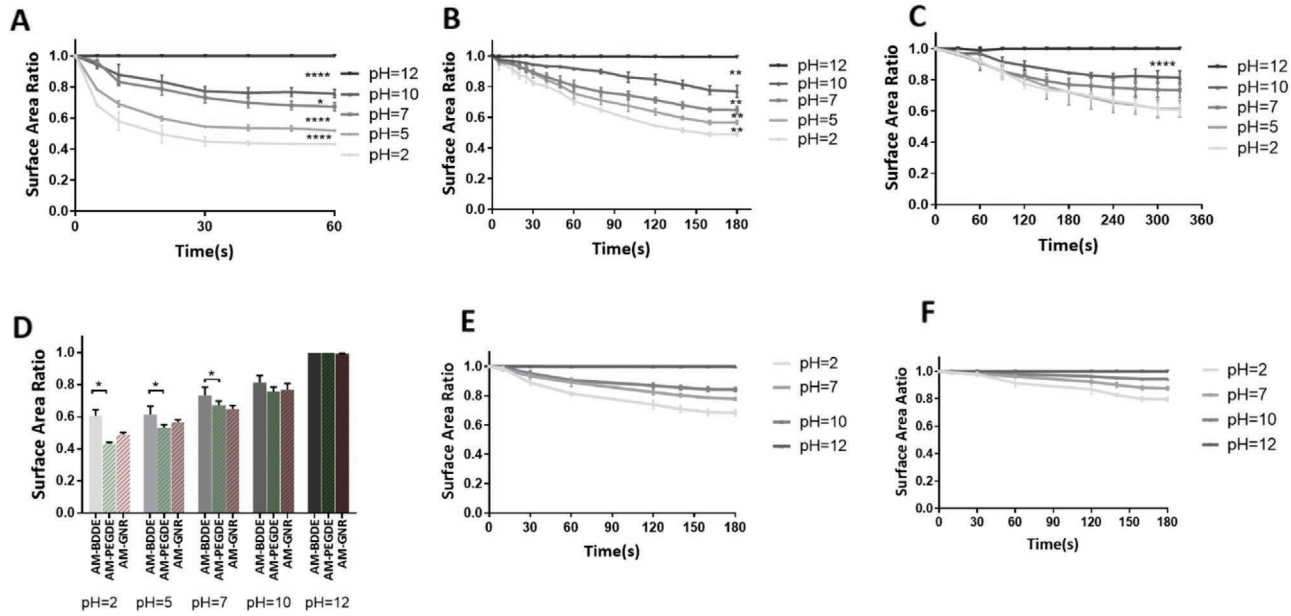

Figure 5. Surface area ratios of A) AM-PEGDE, B) AM-PEGDE-GNR, C) AM-BDDE films at different pH conditions. The kinetics of hydration-triggered actuation and folding of the films increase with decreasing pH and are fastest at a pH of 2; no visible actuation was seen at pH = 12. D) Equilibrium (final) surface area ratios for AM-BDDE, AM-PEGDE, and AM-PEGDE-GNR films. Surface area ratios of Amikagels derivatized with Boc-aspartic acid (BAA) E) BAA-AM-PEGDE and F) BAA-AM-PEGDE-GNR films at different pH conditions. Statistical analysis between groups were determined using one-way ANOVA and Tukey test; p-values < 0.05 were considered statistically significant. For these studies, we carried out $n = 3$ for each condition, and in the figure, $^{*}p$-value < 0.05, $^{**}p$-value < 0.01, $^{***}p$-value < 0.001, $^{****}p$-value < 0.0001.

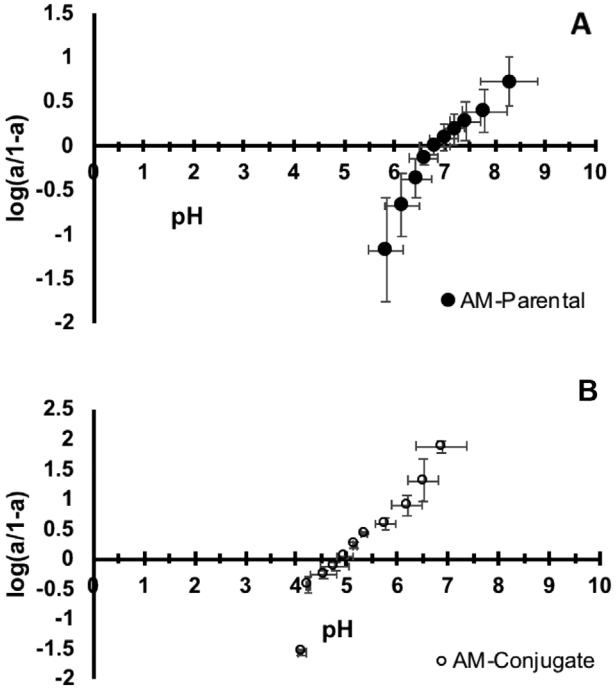

Figure 6. Representative potentiometric titration curve of Parental AM-PEGDE (A) and conjugate, i.e., Boc-aspartic acid-(BAA)-derivatized AM-PEGDE gels (AM-conjugate) (B). Data points are means of $n = 3$ independent experiments. From these, the ionization constant for parental AM-PEGDE was determined as 7.13 ± 0.27 and for the conjugate AM-PEGDE as 4.6 ± 0.36.

investigated. The loss of amine protonation at highly basic pH (i.e., pH 12) results in a loss of actuation and self-folding.

3.4. Hydration-Triggered Actuation and Folding of Derivatized Amikagel Films

In order to investigate the effect of amines on hydration-triggered actuation, Amikagel films were derivatized with Boc-aspartic acid (BAA), lowering the amine content in the derivatized gels. In this approach, amines in the Amikagels were derivatized with the carboxylic acids in BAA, resulting in consumption of amines. Potentiometric titrations (**Figure 6**) of parental and BAA-derivatized AM-PEGDE gels were carried out to investigate properties of the derivatized gel. The ionization constant for AM-PEGDE gel from these potentiometric titrations was determined to be ≈7.13 at 26 °C, indicating that Amikagels can exhibit polyelectrolyte-like behavior,[30,36] which is expected from the rich amine content in the gel. Thus, AM-PEGDE can be significantly protonated at pH conditions below that of 7.13 and deprotonated at pH conditions significantly above 7.13. A deviation from linearity can be observed at pH < 6, which is an indication of a conformational change of the polymer chains under these conditions.[46] This is likely due to the chains adopting an elongated conformation triggered by electrostatic repulsion between the multiple protonated amines.[46] The potentiometric titration curve for BAA-AM-PEGDE is significantly different from that for the AM-PEGDE gel. The ionization constant of BAA-AM-PEGDE was determined to be 4.75 from these data, which is lower than that of AM-PEGDE gels and is indicative of loss of amines and conjugation of the amino acid.

The actuation response of BAA-AM-PEGDE and BAA-AM-PEGDE-GNR films at different pHs was recorded and compared to the parental AM-PEGDE and AM-BDDE films in order to investigate the effect of amines on hydration-triggered self-folding. Although the actuation for the parental films was seen immediately in response to hydration by nanopore water, the conjugated films did not respond as fast (Figure 5E,F); hydration-triggered actuation for BAA-AM-PEGDE and for BAA-AM-BDDE started only after 40 and 60 s, respectively. Although the AM-PEGDE and AM-BDDE reached their equilibrium folding at 40 and 100 s, respectively (Figure 5A,B), it took 3 min for BAA-AM-PEGDE and BAA-AM-PEGDE-GNR films to reach their final folding configuration (Figure 5E,F). Moreover, the extent of maximum folding was significantly lower for BAA-derivatized gels compared to the parental (underivatized) ones (**Figure 7**).

3.5. Computational Modeling

For the base case, we used an aspect ratio of wN/h = 50, $k_\theta = 0.5$, $\zeta = 1.0$, and $q = 1$. **Figure 8**A shows the initial and final configurations, while Figure 8B shows the evolution of the surface "area" ratio, σ, of the film. In the 2D model, σ is defined as the ratio of the maximum span of the film at any given time to its initial span. In the simulations, we assume that the repulsive force is switched on instantly at time $t = 0$. This is somewhat different from experiments, where protonation of the amine groups presumably occurs over time by a slower transport process. It is also plausible that transport induces curling, and is, in turn, affected by the shape of the film. In the computational model, we ignore these nuances to focus primarily on the interplay between elastic and repulsive forces. Due to this initial "shock," we observe a spike in the surface area ratio at short times as the film expands due to repulsion. This is gradually relaxed by deformation, and the surface ratio shrinks to its steady state value.

Within the model, we can understand the driving forces behind the deformation by monitoring the elastic and repulsive contributions (Figure 8C). At time $t = 0$, the total elastic energy $E^s + E^a = 0$, whereas the repulsive energy is at its maximum. For the base case, $E^r = Nq^2 = 25$, initially. The system reacts and seeks to decrease its repulsive energy ($\Delta E^r < 0$) by expanding rapidly, which is manifested in the sharp decrease in ΔE^r at short times, and a corresponding spike in the surface area ratio. Most of this initial deformation is a change in size; by and large, the shape of the film is conserved. Thereafter, the elasticity of the material kicks in, and resists further expansion.

Evolution beyond this point, shifts from changes in size to changes in shape. Due to the constraints placed by the elasticity of the bonds and angles, the material curls up, and adjusts to the repulsive interactions. The dimensionless ratio of repulsive (q^2/l_s^2) to elastic energies ($k_s\, l_s^2 + k_\theta$) for the base case is of order ≈1. Thus, both elastic and repulsive interactions play an important role in the ensuing dynamics. For $m = 1$ and $l_s = 1$, the timescales, $\tau = \sqrt{m l_s^2 / E}$ corresponding to the repulsive, angular, and spring energies are all of order 1. Thus, the unit of time in the simulation is much smaller than that in the experiments. A rough comparison with experimental observations suggests that the unit of time in the simulations corresponds to approximately 10 ms.

To quantify the dynamics of relaxation observed in Figure 8B, we consider the terminal region, well beyond the initial spike ($t > 5000$, in this case) of the surface ratio σ(t), and fit it to an exponential model,

$$\sigma(t) = \sigma_0\, e^{-t/\tau_{relax}} + \sigma_\infty \tag{8}$$

where τ_{relax} is the relaxation time, and σ_∞ is the terminal plateau. The fits obtained using a single exponential mode are excellent for all the calculations performed. The equilibration time is proportional to τ_{relax}, which can therefore

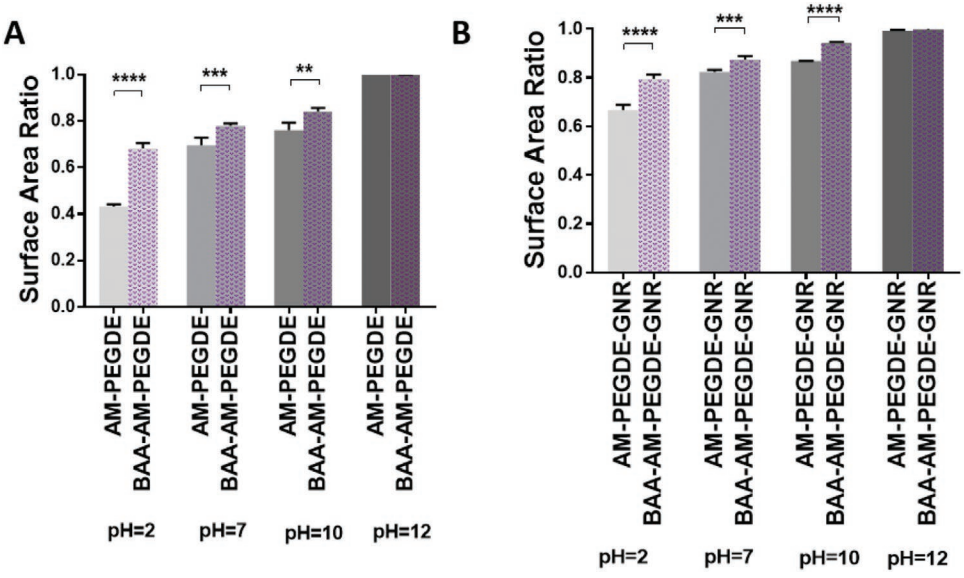

Figure 7. Equilibrium (final) surface area ratios for Boc-aspartic acid-(BAA)-derivatized AM-PEGDE (A) and BDDE (B) compared to the respective unconjugated parental films at different pH values. In the figure, $^{**}p$-value < 0.01, $^{***}p$-value < 0.001, $^{****}p$-value < 0.0001.

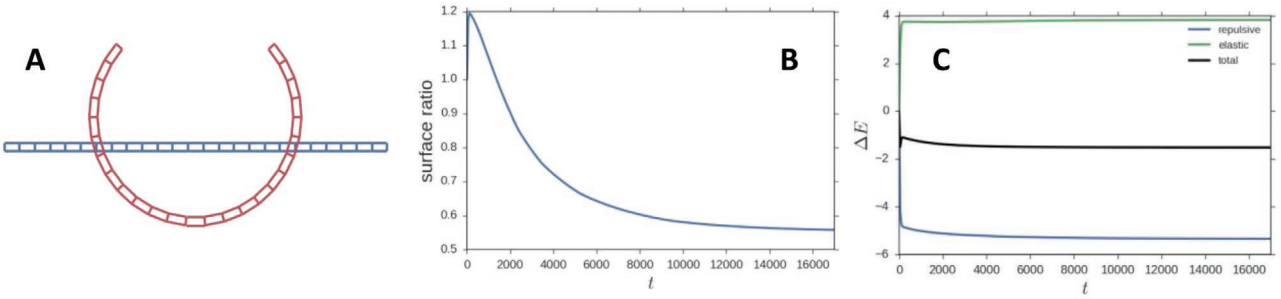

Figure 8. Base case: A) Initial and final state in blue and red, respectively, B) the evolution of the surface ratio with time, and C) evolution of the elastic, repulsive, and total energy of the system.

be thought of as a convenient proxy. Here, $\tau_{\text{relax}} = 3570$, and $\sigma_\infty = 0.55$.

3.6. Dependence on Repulsive Interactions

In the simulations, we can control the strength of the repulsive interaction via the parameter q. Increasing q increases the repulsion between charged neighboring particles, and mimics increased protonation by changing pH in the experiments. Thus, q in the model plays a role analogous to acidity; pH ≈12 and above is similar to $q \approx 0$, where the repulsive driving force is quenched. **Figure 9**A shows the initial and final configuration of the thin film as q is decreased ($q = 0.8$) and increased ($q = 1.2$) with respect to the base case ($q = 1.0$). It is immediately apparent that the final deformation covaries with q, similar to decreasing pH in Figure 5.

The evolution of the deformation for the three cases is tracked in Figure 9B. As q is increased, the initial spike becomes stronger due to the increase in repulsive interactions. The spike is followed by a gradual decay to the plateau value, as the material curls to accommodate repulsion. The surface area ratio curves are fitted to obtain τ_{relax} and σ_∞, which are shown in Figure 9C. As q increases (similar to decrease in pH), σ_∞ changes significantly from 0.73 at $q = 0.8$ to 0.45 at $q = 1.2$. The change in τ_{relax} is more modest; it increases by ≈15–20% over the same range of q.

3.7. Dependence on Thickness

Finally, we study the structure and dynamics that result from varying the thickness of the film. Recall that the increased structural rigidity of the film is modeled by $k_\theta \approx h$. The increased drag, and additional inertia of the system are accounted for with a strong dependence of the drag coefficient with thickness.

Figure 10 is analogous to Figure 9, except that, instead of repulsion, it investigates the dependence of the dynamics and

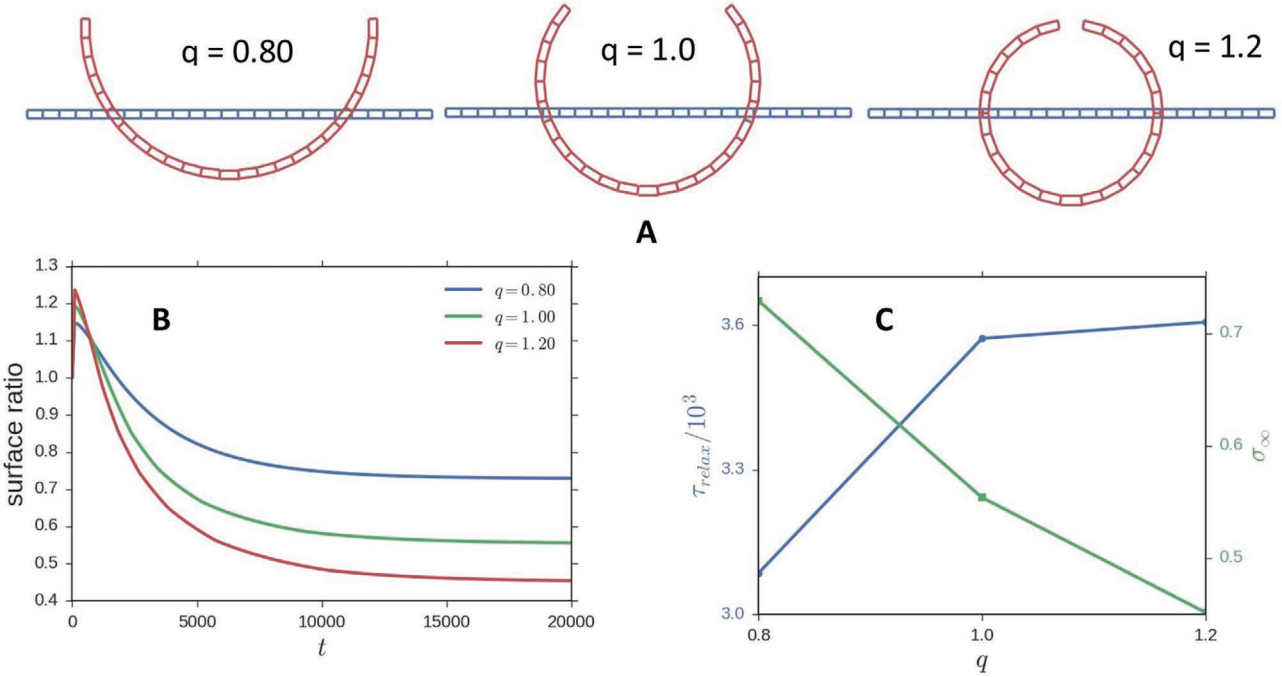

Figure 9. A) Initial and final state in blue and red, respectively, for three different values of q. B) Evolution of the surface ratio for the three cases, and C) the estimated equilibrium time, and plateau.

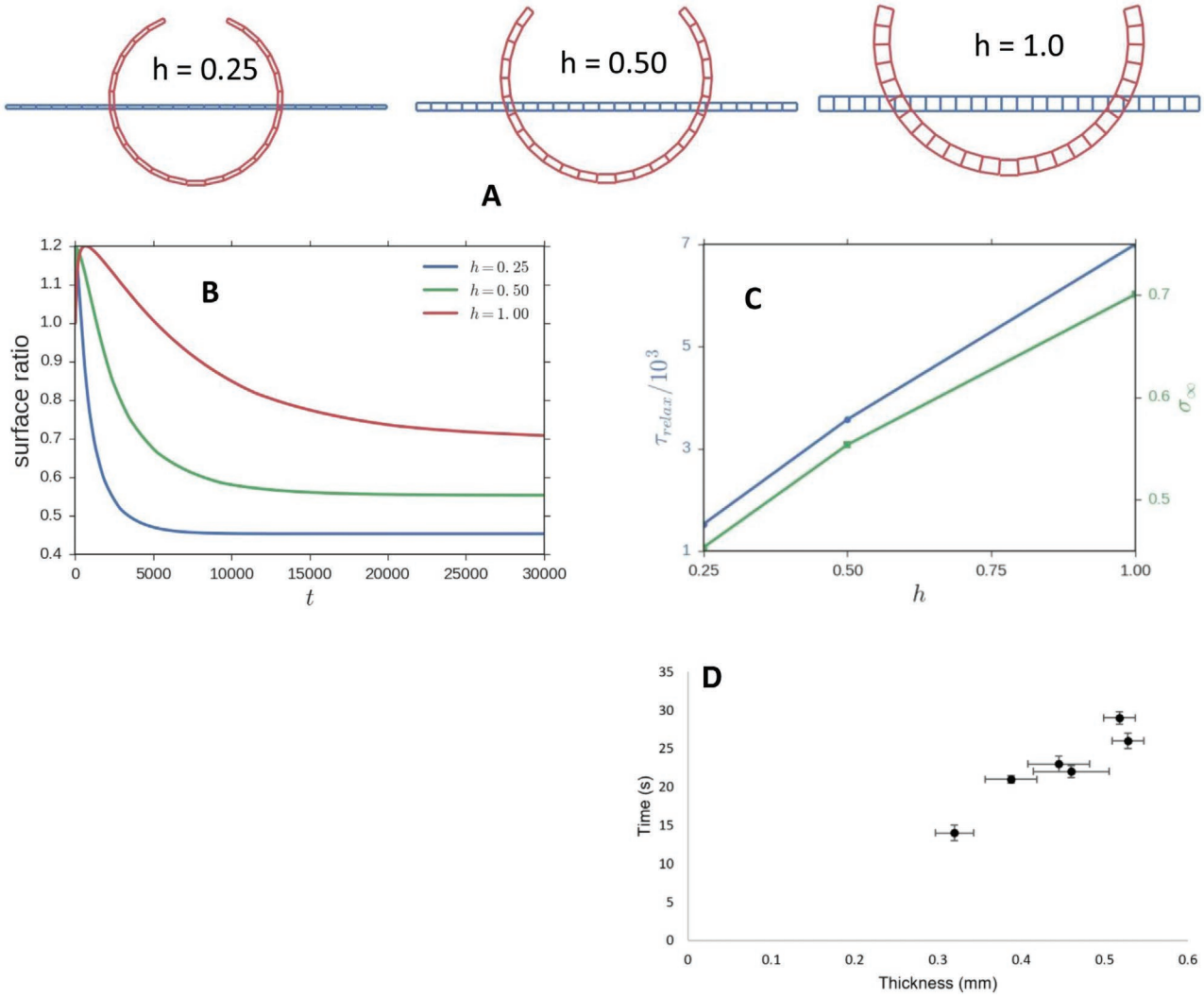

Figure 10. A) Initial and final state in blue and red, respectively, for three different values of thickness, h. From left to right, the aspect ratio decreases from 100 to 25. B) Evolution of the surface ratio for the three cases, and C) the estimated equilibrium time, and plateau. D) Experimental results: time required to reach the final conformation for AM-PEGDE gels increased with increasing thickness of the gel. Values shown are mean ± standard deviation of $n = 3$ independent experiments in each case.

final structure as the thickness, h, is changed. The base case ($h = 0.5$) is shown at the center of Figure 10A. As thickness increases the extent of final deformation decreases. This is evident from Figure 10A,B, which tracks the evolution of the surface ratio. The increase in the structural rigidity with h implies that for a fixed repulsive driving force ($q = 1$, in all these cases), more resistance is offered by the elastic forces, leading to a slower and more muted response. As h increases, σ_∞ increases. The increased sluggishness of the dynamical response is evident in simultaneous increase in τ_{relax} with increasing h. These results are consistent with experimental observations for kinetics of hydration-triggered self-folding as shown in Figure 10D.

4. Conclusions

In this study, we investigated the actuation and self-folding behavior of amine-containing polyelectrolyte gels upon partial hydration as a potential strategy for fabricating diverse shapes. Hydration-triggered actuation of modified and unmodified Amikagel films and their nanocomposites was most prominent under conditions of acidic pH and was completely lost under highly basic pH conditions. This behavior was also seen with other polar solvents (e.g., acetone) but not in presence of hexane, an organic solvent, leading to an unexpected phenomenon of repulsion of polar gels from polar solvents. We reason that the amines present in the gels are immediately protonated upon placement on polar solvents. Repulsion between the increased number of like charges (i.e., protonated amines) within the Amikagel film triggers the actuation in resulting in minimization of the contact area and thus, the interfacial energy.[30] As the chain elongation and contact area minimization happen concurrently, actuation of the films occurs in the form of folding rather than expansion. Folding was more pronounced under acidic conditions, which triggered greater repulsion between the protonated polymer chains in the gel compared to neutral pH. At basic

pH, amines within the Amikagel films are deprotonated, which minimizes electrostatic repulsion and concomitant self-folding. A reduction in protonable amines in the gels also reduced the kinetics and extent of actuation. To our knowledge, this is the first report that demonstrates the spontaneous repulsion of polar (polyelectrolyte) gels from aqueous solvents, resulting in actuation and self-folding behavior that can be employed for the rapid fabrication of a variety of three-dimensional devices.

Supporting Information

Supporting Information is available from the Wiley Online Library or from the author.

Acknowledgements

The authors sincerely thank Dr. Karthik Pushpavanam and Dr. Taraka Sai Pavan Grandhi, then doctoral students in the Rege group, for several helpful discussions. This research was partially supported by NIH (Grant 1R01EB020690) and NSF (CBET-1706268) to K.R., and NSF (DMR-1727870) to S.S.

Conflict of Interest

Dr. Rege is affiliated with a start-up company, Synergyan, LLC.

Keywords

computational modeling, glycoside, polyelectrolyte gels, smart polymers, stimuli responsive

Received: March 23, 2020
Revised: May 3, 2020
Published online: June 11, 2020

[1] M. Jamal, N. Bassik, J.-H. Cho, C. L. Randall, D. H. Gracias, *Biomaterials* **2010**, *31*, 1683.
[2] C. Li, X. Zhang, Z. Cao, *Science* **2005**, *309*, 909.
[3] E. Reyssat, L. Mahadevan, *J. R. Soc., Interface* **2009**, *6*, 951.
[4] a) K. Baek, J. H. Jeong, A. Shkumatov, R. Bashir, H. Kong, *Adv. Mater.* **2013**, *25*, 5568; b) S. Cheng, Y. Jin, N. Wang, F. Cao, W. Zhang, W. Bai, W. Zheng, X. Jiang, *Adv. Mater.* **2017**, *29*, 1700171.
[5] a) J. Mu, C. Hou, H. Wang, Y. Li, Q. Zhang, M. Zhu, *Sci. Adv.* **2015**, *1*, e1500533; b) S. Janbaz, R. Hedayati, A. A. Zadpoor, *Mater. Horiz.* **2016**, *3*, 536.
[6] J. Kim, J. A. Hanna, R. Hayward, C. D. Santangelo, *Soft Matter* **2012**, *8*, 2375.
[7] J. Kim, J. A. Hanna, M. Byun, C. D. Santangelo, R. C. Hayward, *Science* **2012**, *335*, 1201.
[8] R. Fernandes, D. H. Gracias, *Adv. Drug Delivery Rev.* **2012**, *64*, 1579.
[9] T. Yang, R. Ji, X. X. Deng, F. S. Du, Z. C. Li, *Soft Matter* **2014**, *10*, 2671.
[10] G. Huang, Y. Mei, D. J. Thurmer, E. Coric, O. G. Schmidt, *Lab Chip* **2009**, *9*, 263.
[11] Q. Liu, Y. Zhan, J. Wei, W. Ji, W. Hu, Y. Yu, *Soft Matter* **2017**, *13*, 6145.
[12] E. Wang, M. S. Desai, S. W. Lee, *Nano Lett.* **2013**, *13*, 2826.
[13] N. Bassik, B. T. Abebe, K. E. Laflin, D. H. Gracias, *Polymer* **2010**, *51*, 6093.
[14] V. Luchnikov, O. Sydorenko, M. Stamm, *Adv. Mater.* **2005**, *17*, 1177.
[15] A. Richter, G. Paschew, S. Klatt, J. Lienig, K. F. Arndt, H. P. Adler, *Sensors* **2008**, *8*, 561.
[16] D. H. Gracias, *Curr. Opin. Chem. Eng.* **2013**, *2*, 112.
[17] T. G. Leong, A. M. Zarafshar, D. H. Gracias, *Small* **2010**, *6*, 792.
[18] Z. Hu, X. Zhang, Y. Li, *Science* **1995**, *269*, 525.
[19] J. A. H. Jungwook Kim, R. C. Hayward, C. D. Santangelo, *Soft Matter* **2012**, *8*, 2375.
[20] F. M. Andreopoulos, E. J. Beckman, A. J. Russell, *Biomaterials* **1998**, *19*, 1343.
[21] J. Guan, H. He, D. J. Hansford, L. J. Lee, *J. Phys. Chem. B* **2005**, *109*, 23134.
[22] S. K. De, N. R. Aluru, B. Johnson, W. C. Crone, D. J. Beebe, J. Moore, *J. Microelectromech. Syst.* **2002**, *11*, 544.
[23] D. J. Beebe, J. S. Moore, J. M. Bauer, Q. Yu, R. H. Liu, C. Devadoss, B. H. Jo, *Nature* **2000**, *404*, 588.
[24] G. Stoychev, N. Puretskiya, L. Ionov, *Mater. Chem.* **2010**, *20*, 3496.
[25] L. Ionov, *Soft Matter* **2011**, *7*, 6786.
[26] S. Zakharchenko, N. Puretskiy, G. Stoychev, M. Stamm, L. Ionov, *Soft Matter* **2010**, *6*, 2633.
[27] V. Stroganov, S. Zakharchenko, E. Sperling, A. K. Meyer, O. G. Schmidt, L. Ionov, *Adv. Funct. Mater.* **2014**, *24*, 4357.
[28] a) M. Byun, C. D. Santangelo, R. C. Hayward, *Soft Matter* **2013**, *9*, 8264; b) Z. L. Wu, M. Moshe, J. Greener, H. Therien-Aubin, Z. Nie, E. Sharon, E. Kumacheva, *Nat. Commun.* **2013**, *4*, 1586.
[29] P. Nardinocchi, M. Pezzulla, L. Teresi, *Soft Matter* **2015**, *11*, 1492.
[30] X. H. Yuanqing Gu, C. G. Wiener, B. D. Vogt, N. S. Zacharia, *ACS Appl. Mater. Interfaces* **2015**, *7*, 1848.
[31] a) K. N. Lin, T. S. P. Grandhi, S. Goklany, K. Rege, *Biotechnol. J.* **2018**, *13*, 1700701; b) J. Candiello, T. S. P. Grandhi, S. K. Goh, V. Vaidya, M. Lemmon-Kishi, K. R. Eliato, R. Ros, P. N. Kumta, K. Rege, I. Banerjee, *Biomaterials* **2018**, *177*, 27; c) T. S. Pavan Grandhi, T. Potta, R. Nitiyanandan, I. Deshpande, K. Rege, *Biomaterials* **2017**, *142*, 171; d) T. S. P. Grandhi, A. Mallik, N. Lin, B. Miryala, T. Potta, Y. Tian, K. Rege, *ACS Appl. Mater. Interfaces* **2014**, *6*, 18577.
[32] N. Raravikar, A. Dobos, E. Narayanan, T. S. Grandhi, S. Mishra, K. Rege, M. Goryll, *ACS Appl. Mater. Interfaces* **2017**, *9*, 3554.
[33] R. Urie, D. Ghosh, I. Ridha, K. Rege, *Annu. Rev. Biomed. Eng.* **2018**, *20*, 353.
[34] M. R. K. Ali, B. Snyder, M. El-Sayed, *Langmuir* **2012**, *28*, 9807.
[35] C. Huang, K. Rege, J. Heys, *ACS Nano* **2010**, *4*, 2892.
[36] M. V. Kuzimenkova, A. E. Ivanov, I. Y. Galaev, *Macromol. Biosci.* **2006**, *6*, 170.
[37] J. J. Ojeda, M. E. Romero-Gonzalez, R. T. Bachmann, R. G. Edyvean, S. A. Banwart, *Langmuir* **2008**, *24*, 4032.
[38] a) P. J. Flory, J. R. Jr., *J. Chem. Phys.* **1943**, *11*, 521; b) I. Ohmine, T. Tanaka, *J. Chem. Phys.* **1982**, *77*, 5725.
[39] a) H. Li, T. Y. Ng, Y. K. Yew, K. Y. Lam, *Biomacromolecules* **2005**, *6*, 109; b) T. Wallmersperger, K. Keller, B. Kröplin, M. Günther, G. Gerlach, *Colloid Polym. Sci.* **2011**, *289*, 535.
[40] T. Wallmersperger, F. K. Wittel, M. D'Ottavio, B. Kröplin, *Mech. Adv. Mater. Struct.* **2008**, *15*, 228.
[41] D.-W. Yin, F. Horkay, J. F. Douglas, J. J. d. Pablo, *J. Chem. Phys.* **2008**, *129*, 154902.
[42] S. Schneider, P. Linse, *J. Phys. Chem. B* **2003**, *107*, 8030.
[43] D. Frenkel, B. Smit, in *Understanding Molecular Simulation*, Second Edition (Eds: D. Frenkel, B. Smit), Academic Press, San Diego **2002**, 1.
[44] E. C. Achilleos, R. K. Prud'homme, K. N. Christodoulou, K. R. Gee, I. G. Kevrekidis, *Chem. Eng. Sci.* **2000**, *55*, 3335.
[45] T. S. Grandhi, A. Mallik, N. Lin, B. Miryala, T. Potta, Y. Tian, K. Rege, *ACS Appl. Mater. Interfaces* **2014**, *6*, 18577.
[46] a) J. D. Ziebarth, Y. Wang, *Biomacromolecules* **2010**, *11*, 29; b) J. Makowska, K. Baginska, M. Makowski, A. Jagielska, A. Liwo, F. Kasprzykowski, L. Chmurzynski, H. A. Scheraga, *J. Phys. Chem. B* **2006**, *110*, 4451.